AIAA JOURNAL
Vol. 48, No. 12, December 2010

Blockage Effects on the Aerodynamics of a Pitching Wing

Yongsheng Lian*
University of Louisville, Louisville, Kentucky 40292

DOI: 10.2514/1.42215

The blockage effects on the aerodynamic characteristics of stationary wings have been extensively studied, both numerically and experimentally. However, the effects on flapping wing aerodynamics have not been fully explored. In this paper, the blockage effects on the aerodynamics of a pitching wing are investigated using a numerical approach. The flowfield is described by solving the Navier–Stokes equations on an overlapping grid. The wing motion is handled by a moving overlapping grid method. Force histories at different blockage ratios and reduced pitching frequencies are compared. Simulations show that the pitching motion can mitigate the blockage effects: the higher the reduced frequency, the more minimal the blockage effects. In addition, the sidewall effects are studied. It is demonstrated that sidewalls can lead to a strong spanwise variation in the flowfield, and the variation is further extenuated by the existence of a leading-edge vortex.

Nomenclature

A_p	=	oscillation amplitude
b	=	span
c	=	chord length
C_D	=	drag coefficient per unit span
C_L	=	lift coefficient per unit span
C_T	=	thrust coefficient per unit span
D	=	diameter of a circular cylinder
f	=	pitching frequency
k	=	reduced frequency, $\pi f c/U_0$
KC	=	Keulegan–Carpenter number, $2\pi A_p/D$
Re	=	Reynolds number, $U_0 c/\nu$
S	=	reference cross-sectional area of wing
T	=	period, $2\pi/\omega$
U_0	=	reference velocity, typically freestream velocity
β	=	Stokes parameter, $\rho D^2/(\mu T)$
θ	=	pitching angle of attack
θ_0	=	pitching amplitude
μ	=	viscosity
ν	=	kinematic viscosity
ρ	=	fluid density
ω	=	oscillating circular frequency

Introduction

MICRO Air Vehicles (MAVs) have drawn growing interest from both engineering and science societies because of their potential military and civilian applications [1]. Typically, an MAV has a maximum dimension of 15 cm or less and a flight speed of less than 15 m/s. Because of their small size and low flight speed, MAVs operate at low Reynolds numbers ($Re \leq 10^4$), and flow around MAVs is characterized with rich unsteady phenomena. Consequently, the principles that have guided us for aircraft design cannot be directly applied to MAV design, since these principles are calibrated for steady-state high-Reynolds-number flight. In MAV design, one of the most challenging issues is to generate sufficient lift to keep the vehicle airborne. Recent research has identified that flapping wings take advantage of unsteady mechanisms to enhance their lift generation capability [2,3]. This, together with other characteristics such as gust resistance [4], makes flapping wings the most promising candidates for MAV design. In the study of flapping wings, the following issues have been extensively discussed and studied:

1) To what extent does flapping wing aerodynamics need to be handled by unsteady models? While flapping motions and associated fluid flows are intrinsically time dependent, at high frequency, the noncirculatory effect can dominate, and the classical attached flow models and quasi-steady models seem to be able to capture substantial essence for certain flyers [5].

2) To what extent can the lift be expressed as an analytical function of the wing kinematics? That is, when are the aerodynamic forces closed-form functions of the angle of attack and its first few derivatives?

3) To what extent does the Reynolds number affect the flapping wing performance? The drag polar and lift curve slope of fixed airfoils at $Re < 10^5$ are profoundly affected by laminar flow separation, exhibiting the so-called drag bulge. These phenomena are strongly dependent on Reynolds number, airfoil surface roughness, and ambient turbulence intensity. It is not clear whether flapping wings will show similar patterns.

4) What is the role of each parameter in flapping wing performance? The Strouhal number, reduced frequency, plunge amplitude, pivoting point, and phase lag all affect the flapping wing performance. Identifying their individual roles is critical in the MAV design. Unfortunately, because the exploration of such a wide space is a formidable task, the question is still not clear.

Blockage and sidewall effects have been extensively studied for stationary wings. However, their effects on flapping wing aerodynamics have not drawn enough attention. In flapping wing experiments, especially in water-tunnel experiments, wings can be in the close proximity of the top and bottom surfaces. There is evidence that blockage and sidewalls can affect the flapping wing aerodynamics. For example, Ol [6] observed strong three-dimensional (3-D) flow behavior in his two-dimensional (2-D) experimental setup. In his experiment, an aspect-ratio-3 wing was mounted wall to wall with a small clearance (equivalent to boundary-layer thickness) between the wingtip and sidewall. The wing experienced a plunge motion with the amplitude of $0.05c$. Ol observed that the spanwise flow in the shed vortices became stronger with increasing reduced frequency. His experiment also demonstrated that the spanwise flow was not due to the intrusion of the rig's centered-mounted plunge rods.

It is known that sidewalls can produce 3-D effects, of which a typical example is the spanwise flow in shed vortices in the wake [6]. When flow passes a cylinder, the flow shows 3-D vertical instability in the wake. Williamson [7] attributed this instability to the particular boundary conditions at the spanwise ends of the cylinder. However, the spanwise velocity in the wake is typically much smaller than the

Received 15 November 2008; revision received 23 July 2010; accepted for publication 1 August 2010.

*Assistant Professor, Mechanical Engineering Department; y0lian05@louisvill.edu. Senior Member AIAA.

freestream velocity. In Ol's experiment [6], the spanwise velocity is comparable to the freestream velocity. Obviously, this large variation cannot be readily modeled by the flow instability theory.

Flapping wing simulations typically use large computational domains to mitigate the blockage effects. This is hardly true for the experiment. For example, Dickinson et al. [8] tested a 25-cm-long model wing immersed in a $1 \times 1 \times 2$ m tank filled with mineral oil. At the closest position, the wingtip came within 22 cm of the top surface and 18 cm from the sidewalls. Ol [6] tested a flapping rectangular wing in a water channel. At the closest point, the wing came within less than $2c$ of the top and bottom surfaces. Koochesfahani [9] experimentally studied a pitching NACA0012 wing. The experiment was done in a low-speed channel with a 50-cm-wide and 76-cm-deep test section. The test wing had a chord of 8 cm. The experiment was run with pitch amplitudes of 2 and 4° and a reduced frequency ranging from 1.0 to 12. He calculated the mean thrust coefficient by measuring the momentum of the time-averaged velocity profiles on a control volume. His results showed noticeable difference from the simulated solutions by others, especially at high reduced frequencies. Ramamurti and Sandberg [10] stated that Koochesfahani's experiments [9] increasingly overpredicted the thrust with increasing pitching frequency, citing the ignorance of the unsteady effects and pressure differences on the control volume. Bohl and Koochesfahani [11] demonstrated that inclusion of the unsteady velocity quantities could significantly improve experimental prediction of thrust for high-frequency low-amplitude pure-plunge cases. Lian and Ol [12] performed a combined experimental and numerical study of a pitching flat plate. Using the same domain as the experiment, the simulation predicted the same maximum lift coefficient as the experiment; using a larger domain, the simulation predicted a much higher maximum lift coefficient.

A thorough understanding of the blockage and sidewall effects is critical in the study of flapping wing aerodynamics. It not only guides us to properly design the experiment and make blockage corrections but helps us interpret the disparity between the numerical and experimental data so improved numerical models can be proposed. In this paper, we numerically study the blockage and sidewall effects on a pitching wing. We compare the force histories at different blockage ratios and reduced frequencies. Since flapping wing performance is affected by various factors, such as wing kinematics and Reynolds number, the effects of blockage and sidewall may vary from case to case. We are not intent to exhaust all the combinations but to quantitatively demonstrate the blockage and sidewall effects on pitching wing aerodynamics.

Numerical Methods

We solve the time-dependent incompressible Navier–Stokes equations with finite differences on a curvilinear overlapping grid. The method is fourth-order accurate in space and uses the momentum equations for the velocity coupled to a Poisson equation for pressure [13]. Time stepping is accomplished using a second-order-accurate Adams predictor–corrector method [14].

We use a moving overlapping grid approach [15] to dynamically update the computational grid to accommodate the wing motion. The overlapping grid uses boundary-conforming structured grids to achieve high-quality representations of boundaries. It employs Cartesian grids as the background grids so that the efficiencies inherent with Cartesian grids can be exploited. The irregular boundary associated with standard Cartesian grid methods takes the form of the interpolation boundary between overlapping grids.

Results and Discussions

Code Validation

We first validate our code to establish the confidence in its prediction capability in the study of moving body problems. The case chosen is a transversely oscillatory circular cylinder in stationary flow. The circular cylinder has a diameter of D, and its motion and velocity are described as follows:

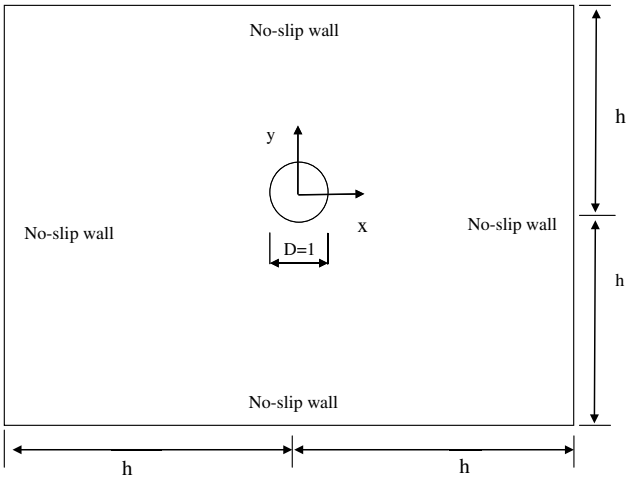

Fig. 1 Computational setup for the transversely oscillating circular cylinder.

$$x(t) = -A_p \sin(\omega t) \tag{1}$$

$$\dot{x}(t) = -A_p \omega \cos(\omega t) = -U_m \cos(\omega t) \tag{2}$$

where A_p is the oscillation amplitude, ω is the oscillation circular frequency, and U_m is the maximum oscillation speed. Tatsuno and

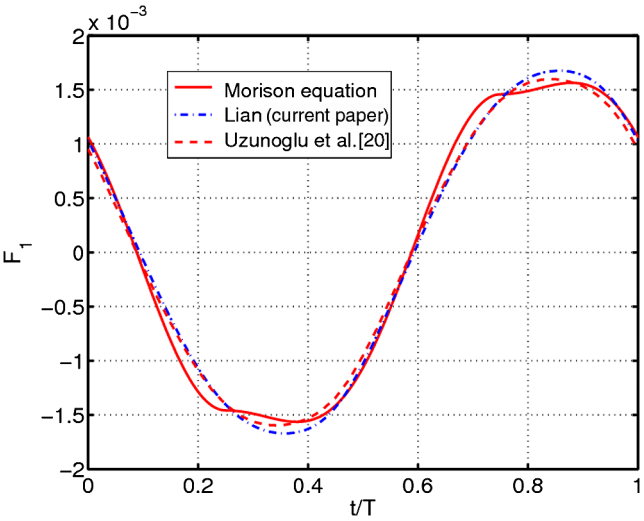

Fig. 2 Inline force [in Eq. (5)] computed over a 2-D circular cycle at $Re = 100$ and $KC = 5$.

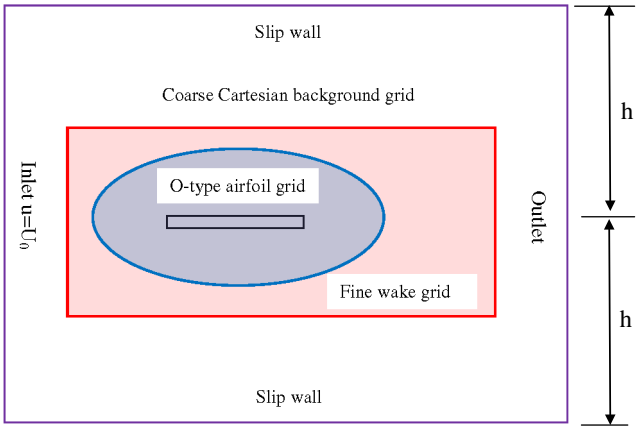

Fig. 3 Boundary conditions used in the simulation of flapping wing.

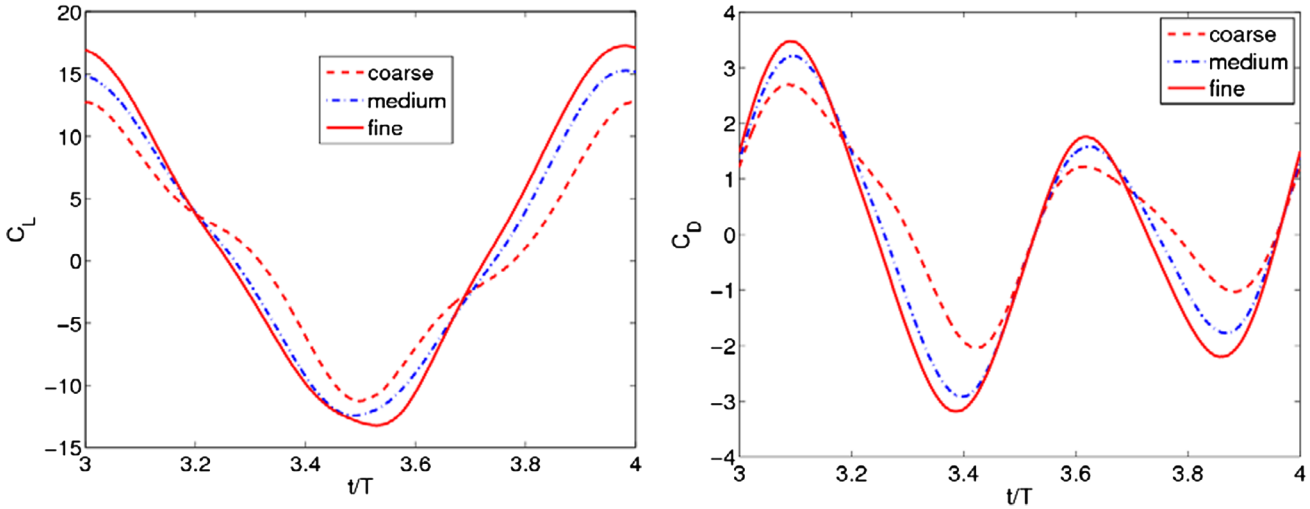

Fig. 4 Grid sensitivity test for a pitching airfoil ($h = 2c$, $Re = 10,000$, $k = 3.93$, and $\theta_0 = 21.5°$).

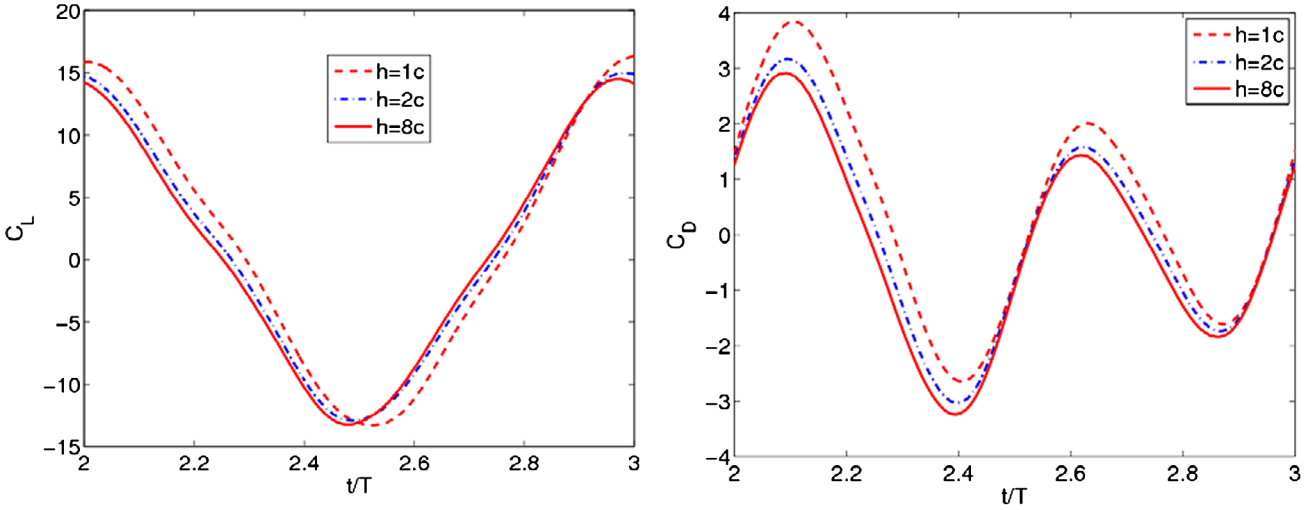

Fig. 5 Blockage effect on the aerodynamic forces of a pitching airfoil ($Re = 10,000$, $k = 3.93$, and $\theta_0 = 21.5°$).

Bearman [16] illustrated that the complexity of the vortex patterns were determined by the following two parameters:

$$KC = \frac{U_m T}{D} \tag{3}$$

$$Re = \frac{\rho U_m D}{\mu} \tag{4}$$

where $T = (2\pi/\omega)$ is the oscillation period, ρ is the fluid viscosity, and μ is the viscosity. In our study, the Reynolds number Re is 100 and the KC number is 5. Under this condition, two vortices shed symmetrically per half cycle, and flow is essentially 2-D [16,17].

The inline unsteady force acting on the cylinder per unit span can be modeled with a semiempirical Morison equation [18,19]:

$$F_1(t) = -\tfrac{1}{2}\rho D C_D \dot{x}|\dot{x}| - \tfrac{1}{4}\rho\pi D^2 C_I \ddot{x} \tag{5}$$

where C_D and C_I denote the drag coefficient and added mass, respectively. For an Re of 100 and a KC of 5, Dutsch et al. [17] used a finite volume method to determine that $C_D - 2.09$ and $C_I = 1.45$. Another numerical analysis by Uzunoglu et al. [20] showed a slightly different value of $C_D = 2.10$.

The computational setup is shown in Fig. 1. The center of the cylinder is initially at the origin ($x = 0$ and $y = 0$). The no-slip boundary condition is imposed on all outer boundaries. Our tests show that a domain size of $h = 6D$ is sufficiently large enough that the imposed boundary conditions influence the forces insignificantly.

In Fig. 2, the inline force variation with time is presented. The computed result is compared with the semiempirical prediction of Eq. (5) and the numerical result of Uzunoglu et al. [20]. A reasonable agreement exists between the inline force from three analyses.

Pitching Wing Test: Grid Sensitivity Analysis

The case studied here is a SD7003 airfoil[†] experiencing pitching motion about the quarter-chord position from the leading edge. The pitching motion is described as follows:

$$\theta(t) = \theta_0 \cos\left(\frac{2kU_0 t}{c}\right) + 4° \tag{6}$$

where θ_0 is the pitching amplitude, k is the reduced frequency, U_0 is the freestream velocity, and c is the airfoil chord. In our test, θ_0 is 21.5°, k is 3.93, and the Reynolds number Re based on the chord and freestream velocity is 10,000. At this Reynolds number, we assume flow is laminar.

The computational configuration is shown in Fig. 3. It is based on the experimental setup [4] in which the wing was $2c$ away from the top and bottom surfaces at its starting point. The slip boundary condition is applied on the top and bottom surfaces. The Dirichlet boundary condition is applied at the inlet, and a zero gauge pressure

[†]Data available at http://www.ae.illinois.edu/m-selig/ads/coord_database.html#S [retrieved July 2010].

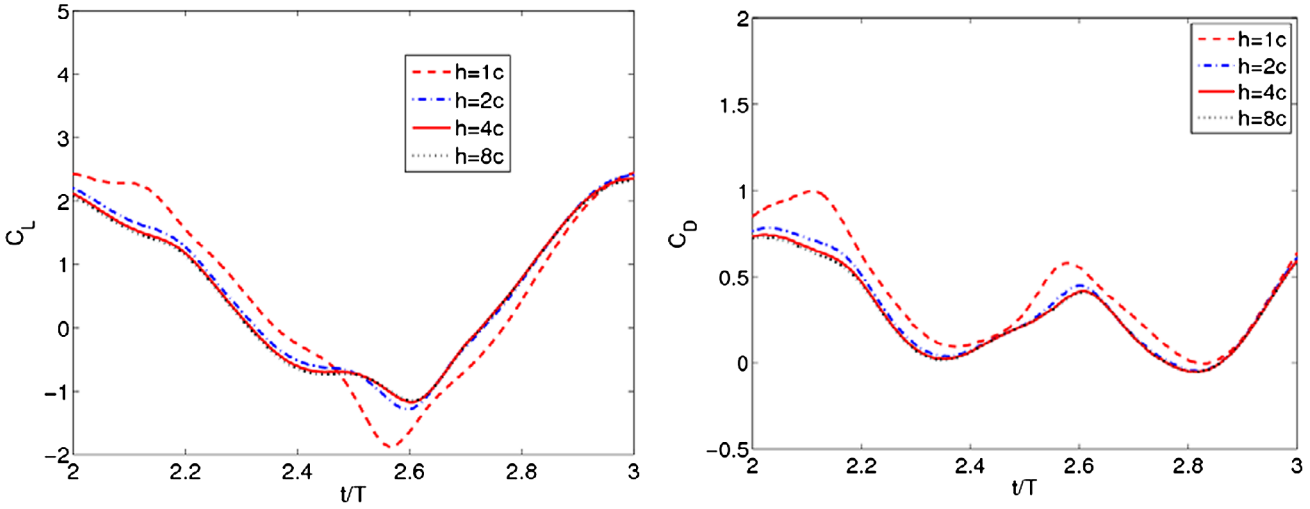

Fig. 6 Blockage effect on the aerodynamic forces of a pitching airfoil ($Re = 10,000$, $k = 1.0$, and $\theta_0 = 21.5°$).

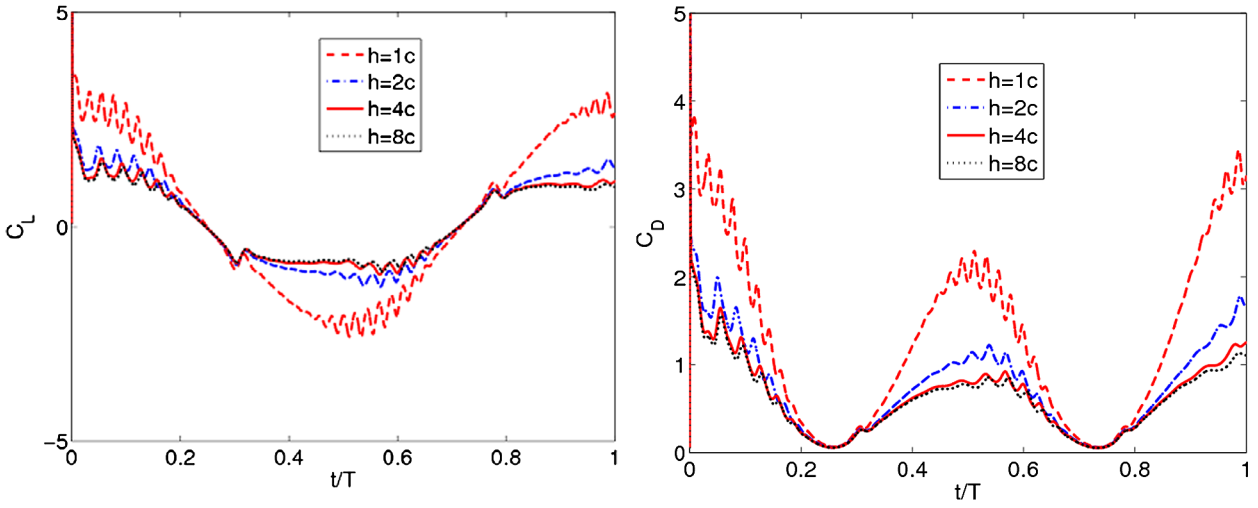

Fig. 7 Blockage effect on the aerodynamic forces of a pitching airfoil ($Re = 10,000$, $k = 0.03$, and $\theta_0 = 45°$).

boundary condition is applied at the outlet. An O-type grid is generated around the airfoil using a hyperbolic grid generator embedded in the Overture package.[‡] To better capture flow structure in the wake region, a fine wake grid is added. The background grid is a coarse uniform Cartesian grid.

Strictly speaking, a no-slip boundary condition should be applied on the top and bottom surfaces to model the wall effect. However, such an arrangement requires an extremely fine grid near the surfaces to capture the boundary-layer development along the channel. Such a fine grid inevitably increases the computational cost. On the other hand, a coarse grid near the top and bottom surfaces will reduce the computational cost but will predict a thicker boundary layer that can exaggerate the blockage effect. To balance the solution accuracy and computational cost, we use the slip boundary condition. Such an arrangement essentially simulates flow in the core frictionless region in the channel. Because the boundary-layer thickness will be thin at this Reynolds number, the setup is a good approximation of the experiment.

We notice that the distance upstream to the airfoil influences the forces more than the distance downstream to the airfoil. But as the upstream distance is more than $12c$ and the downstream distance is more than $6c$ away from the airfoil, their influence diminishes. An upstream distance of $12c$ and a downstream distance of $6c$ are used throughout this paper.

[‡]Data available at https://computation.llnl.gov/casc/Overture/ [retrieved October 2010].

The computed forces are sensitive to the grid density in the wake region and near the airfoil surface and the distribution of the airfoil grid, signaling the importance of viscous effect. The domain size and grid density of the O grid are carefully adjusted so that the O-grid density matches the wake grid density in their overlapping region. We find that such an arrangement can capture the vortex evolution (hence force variation) without using excessive grid points in the circumstantial direction around the airfoil. A hyperbolic stretching is applied to the O grid to ensure there are at least 10 grid points in the boundary layer. In most cases, our simulations reach periodic after the second cycle. The sensitivity analysis results in the third cycle are presented in Fig. 4. Based on our analysis, the medium density grid is used in our study.

Blockage Effect at Different Reduced Frequencies

The force histories at k of 3.93 and θ_0 of 21.5° are shown in Fig. 5. Three computational domains are tested. As the domain size increases from $1c$ to $2c$, both the lift and drag show noticeable differences. However, a further increase in the domain size does not result in significant change. Force histories at a low reduced frequency of 1.0 are shown in Fig. 6. Compared with the high-frequency case (Fig. 5), the difference in lift and drag between $1c$ and $2c$ is larger. However, the results from $2c$ and $4c$ are indistinguishable. We further test a very low frequency of 0.03. In this case, flow passes the wing about 100 times during each pitch cycle. At this low frequency, we observe some difference between $2c$ and $4c$ (Fig. 7). Force histories over a stationary wing at an angle of attack of

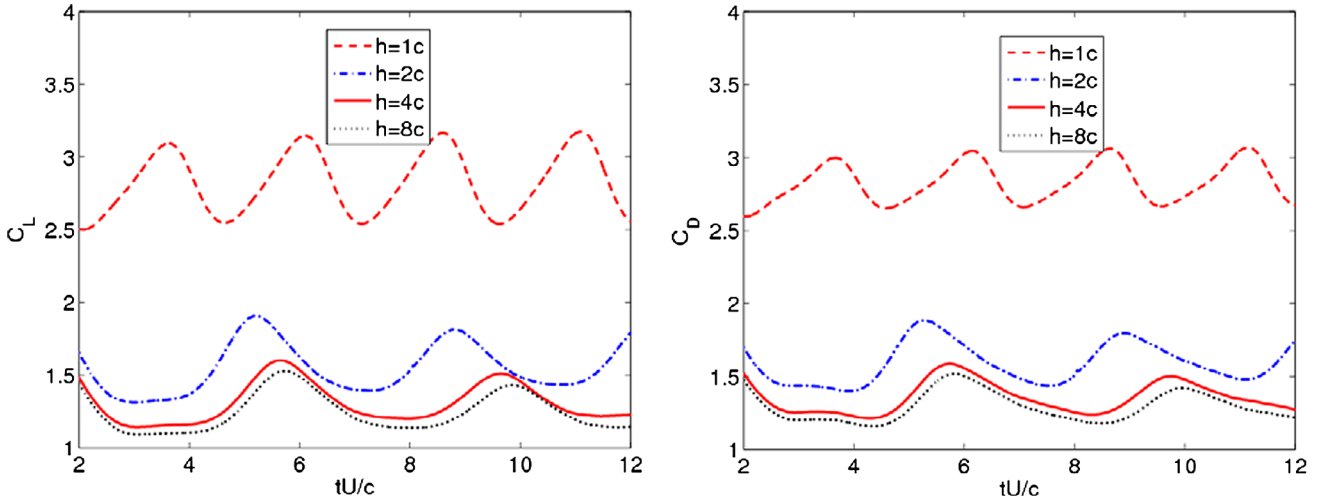

Fig. 8 Blockage effect on the aerodynamic forces of a stationary airfoil at an angle of attack of 45° ($Re = 10,000$).

45° are shown in Fig. 8. The difference between $2c$ and $4c$ is clear. Based on these tests, we conclude that the pitching motion can mitigate the blockage effect: the higher the reduced frequency, the less the blockage effect. However, just like the high-frequency case, the blockage effect is negligible at the modest reduced frequency ($k \geq 1$) once h is larger than $2c$.

Blockage Effect at Different Pitch Amplitude

To further understand the blockage effect, we increase the pitching amplitude from 21.5 to 45°. Comparing Figs. 6 and 9 we can see that, for the domain size of $1c$, the blockage effect is more severe at a higher pitch amplitude. However, the blockage effect diminishes once the domain size is larger than $2c$.

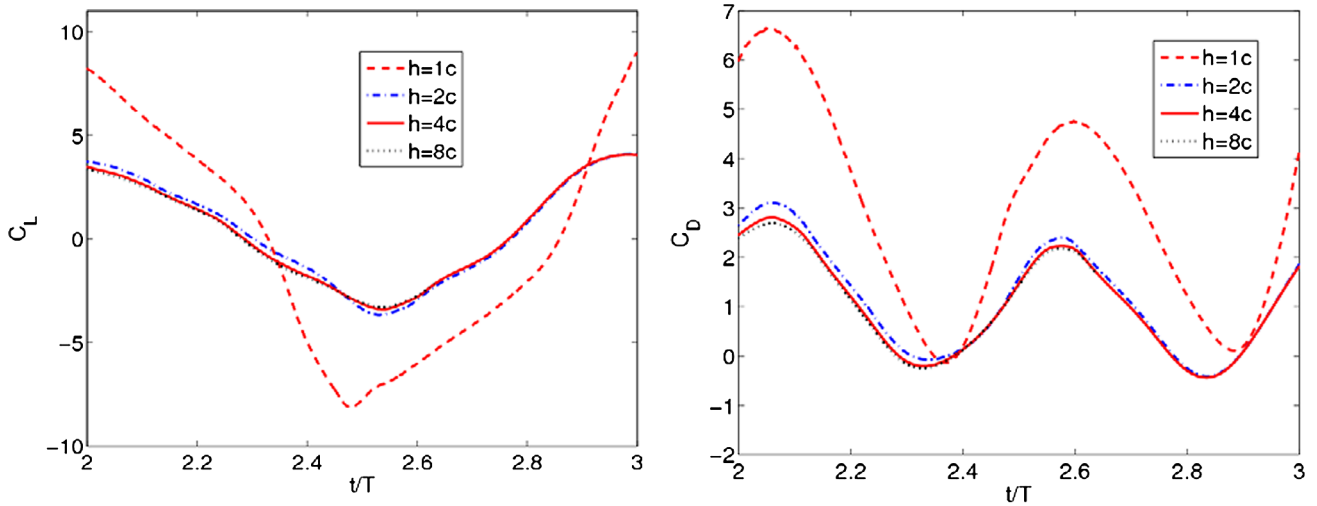

Fig. 9 Blockage effect on the aerodynamic forces of a pitching airfoil ($Re = 10,000$, $k = 1.0$, and $\theta_0 = 45°$).

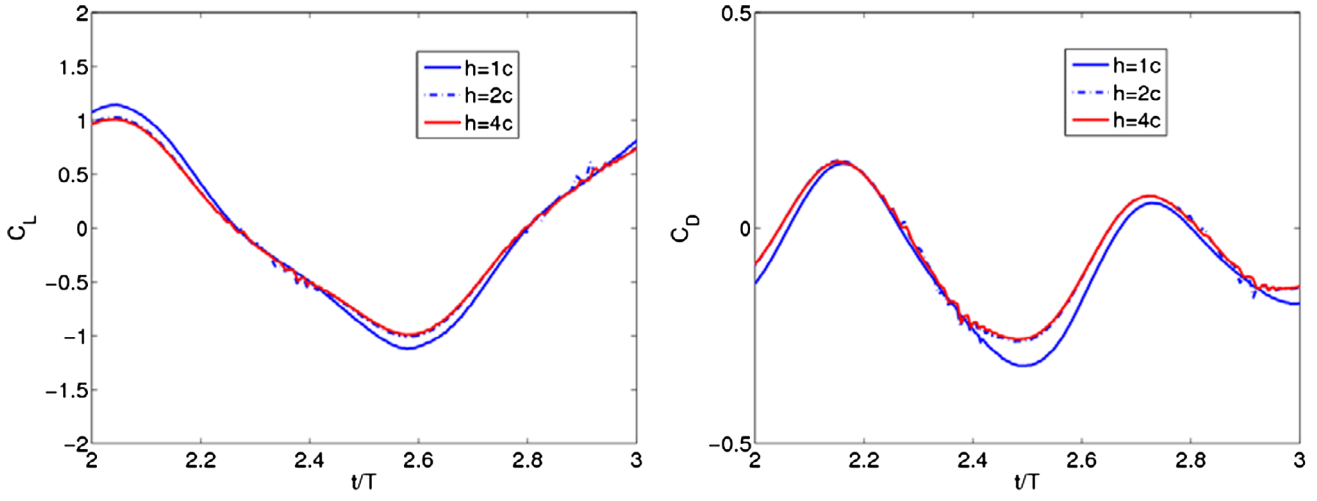

Fig. 10 Blockage effect on the aerodynamic forces of a pitching airfoil with no freestream ($k = 1.0$, and $\theta_0 = 21.5°$).

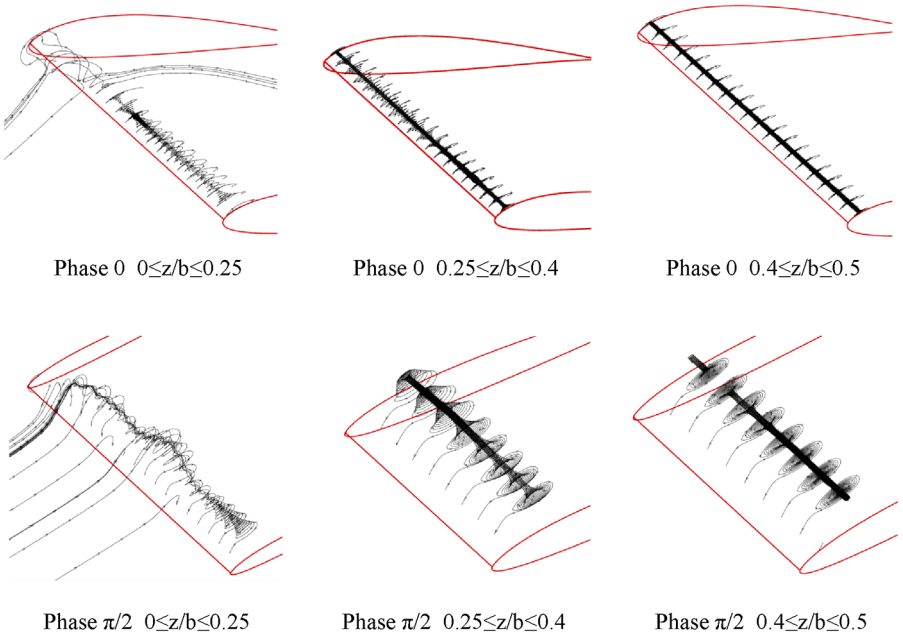

Fig. 11 Streamlines near the upper surface of the pitching wing with side, top, and bottom walls: a) $0 \le z/b \le 0.25$, b) $0.25 \le z/b \le 0.40$, and c) $0.40 \le z/b \le 0.50$ (z is the distance from the wingtip, and b is the wingspan).

Blockage Effect for Hovering Flight

Figure 10 shows the results with no freestream. There is some difference in lift and drag between the domain sizes of $1c$ and $2c$. But the lift and drag histories are almost identical between $h = 2c$ and $h = 4c$. Comparing force histories without freestream (Fig. 10) and those with freestream (Fig. 6) reveals that the top and bottom walls have less influence on the aerodynamics when there is no freestream.

Three-Dimensional Effect

Now we study the spanwise flow variation. The SD7003 wing had an aspect ratio of three and was mounted wall to wall in the water tunnel. The clearance between the wingtip and the sidewalls was less than the boundary-layer thickness. In the simulation, the sidewalls and the top and bottom walls were simulated. However, the clearance between the wingtip and the sidewall was not modeled. The side view of the computational setup was the same as that described in Fig. 4a. The wing motion followed Eq. (6), and the Reynolds number was 10,000. Figure 11 shows the streamlines near the upper surface at phases 0 and $\pi/2$. Here, phase 0 refers to $\alpha = 4°$ and when the trailing edge is about to start moving down. The streamlines revealed complex flow patterns along the span. From wingtip to 25% inbound (Fig. 11a), flow was circulated away from the wall, but the vortex structure was irregular. From 25 to 40%, there was a vortex tube, and flow was circulated toward the wall. From 40% to middle span, flow moved toward the middle span again. Analyzing the spanwise velocity near the upper surface of the wing reveals that, from phase 0 to phase $\pi/2$, the high-velocity region ($v/U_0 > 0.4$) grew and moved toward the middle span, indicating increasing spanwise variation from phases of 0 to $\pi/2$.

From the boundary-layer theory, we know that, within the boundary layer, the transverse pressure gradient is negligible. Here, we can assume a constant pressure along the span when the wing remains stationary. However, this constant distribution changes if the wing is undergoing flapping motion, especially when the reduced frequency is high (Fig. 12a). When the wing moves away from its original position, it leaves a vacancy that must be filled by nearby fluid. Near the sidewalls, the fluid is nearly stagnant because of

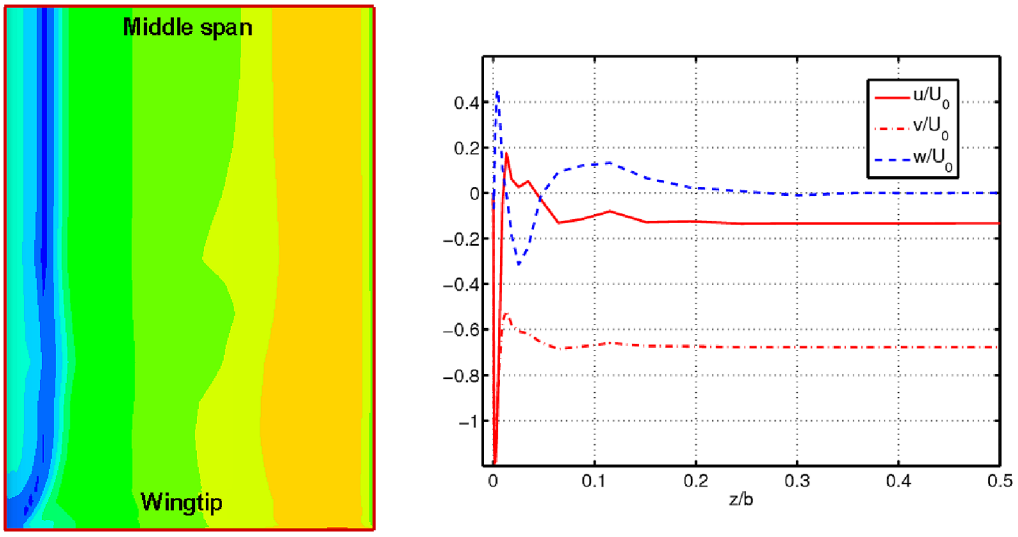

a) b)

Fig. 12 Pressure and velocity distributions along the span close to the upper surface. A strong leading vortex exists on the upper surface. Components u, v, and w are the velocity components in the streamwise, normal, and spanwise directions, respectively.

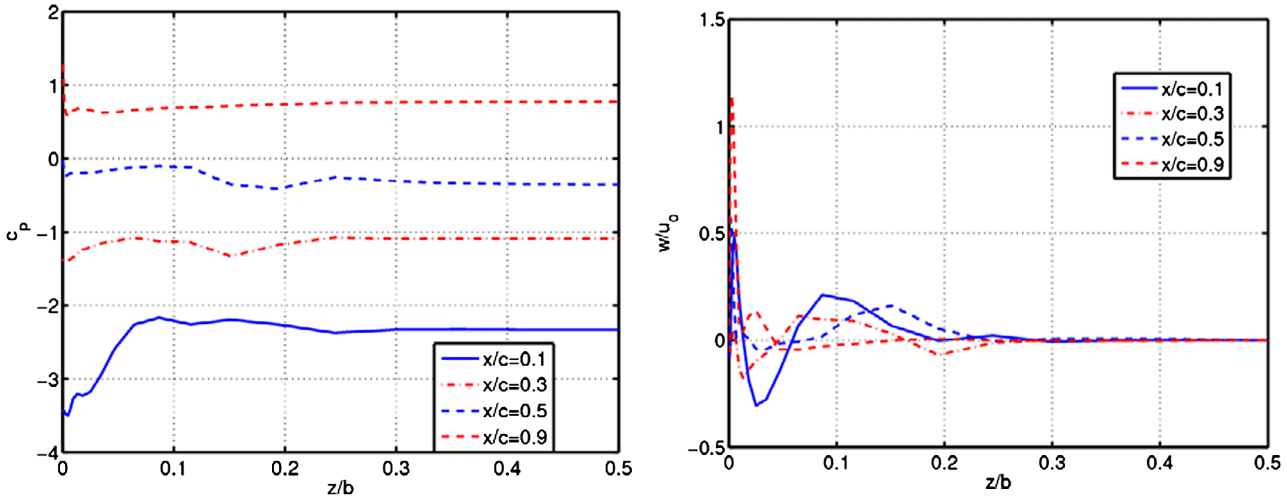

Fig. 13 Propagation of velocity and pressure disturbances toward the middle span on the upper surface. When there is a strong leading-edge vortex, the pressure and velocity show strong variation along the span.

viscous friction and cannot fill the space as quickly as fluid outside the boundary layer. Therefore, fluid from outside the boundary tends to be squeezed into the boundary in order to fill the vacancy. This causes overshoots in the velocity and pressure profiles near the sidewalls (Fig. 12b). These overshoots propagate downstream and move toward the middle span (Fig. 13). From this reasoning, we can conclude that the higher the reduced frequency, the more severe the spanwise variation.

The disturbance along the spanwise variation is further amplified by the vortex tube when flow travels downstream. From the phase of

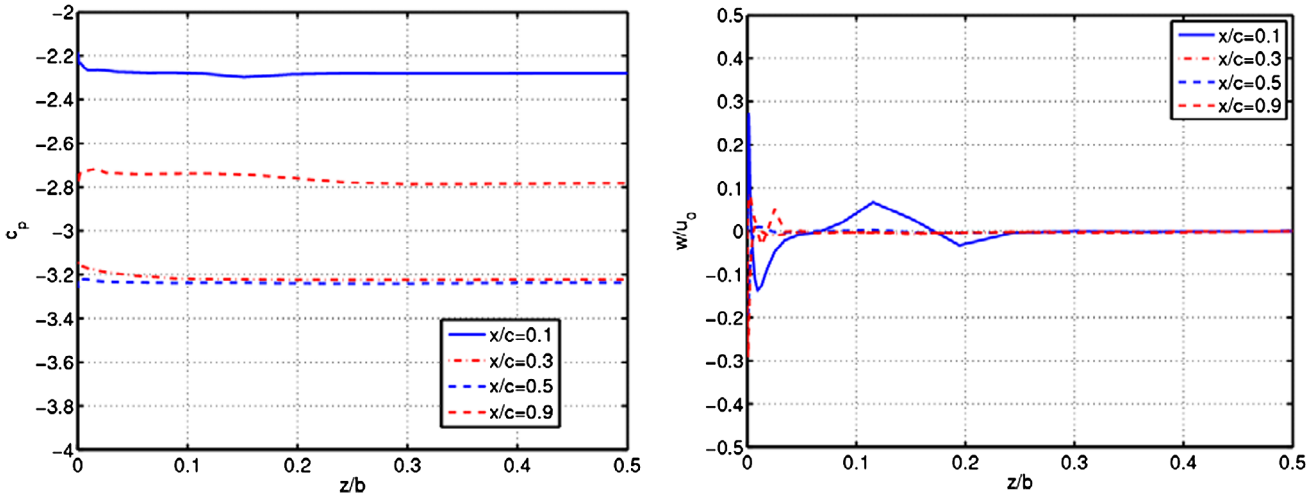

Fig. 14 Velocity and pressure distributions at different streamwise locations on the lower surface. When there is no strong leading-edge vortex, the pressure and velocity are nearly constant along the span, except near the leading edge.

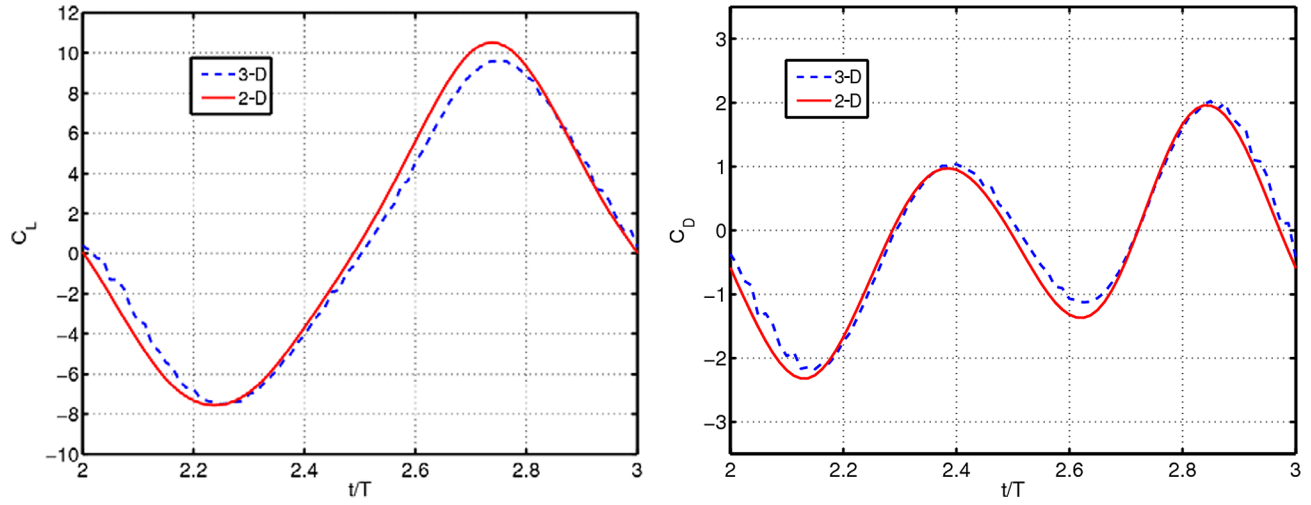

Fig. 15 Comparison of force histories between 2-D simulation and 3-D simulation, with sidewalls and freestream velocity.

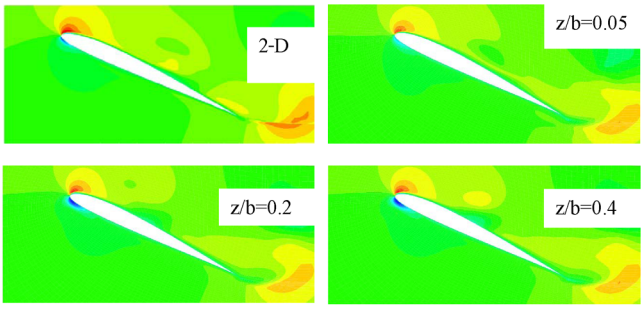

Fig. 16 Comparison of streamwise velocity contours between 2-D and 3-D at phase 0.

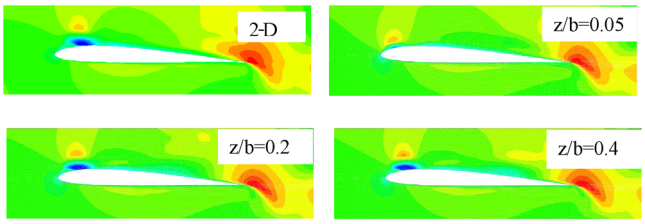

Fig. 17 Comparison of streamwise velocity contours between 2-D and 3-D at phase $\pi/2$.

0 to the phase of $\pi/2$, there is a strong vortex structure near the leading edge on the upper surface. However, during the same period, because there is not such a strong vortex on the lower surface, the pressure and velocity are almost constant along the span on the lower surface, except near the leading edge (Fig. 14).

Now, we compare the force and flowfield between the 3-D wing and 2-D airfoil, both with top and bottom walls. It is clear from Fig. 15 that neither the lift nor drag coefficients showed significant difference between the 2-D and 3-D results. At the phase of 0, the streamwise velocity profile near the sidewall ($z/b = 0.05$) was clearly different from the 2-D solution (Fig. 16). However, the profile was similar to the 2-D profile from $z/b = 0.25$ to the middle span. The same conclusion held at phase $\pi/2$ (Fig. 17).

Conclusions

The blockage effect and sidewall effect on a pitching wing was studied. Tests showed that the blockage effect can significantly affect the wing aerodynamics when the domain size is small ($h = 1c$). For a large domain ($h \geq 2c$), the blockage effect is observed at low reduced frequency cases, but no noticeable blockage effect is observed at modest reduced frequencies. Tests also showed that the dynamic motion can mitigate the blockage effect: the higher the reduced frequency, the less the blockage effect. For the pitching wing case, a larger pitch amplitude leads to more blockage effect. The sidewalls cause strong spanwise variation in both pressure and velocity. This spanwise variation is further amplified by the existence of a leading-edge vortex. When there is no leading-edge vortex, the sidewalls affect regions close to the leading edge, and further downstream, flow is nearly 2-D.

Acknowledgment

This work is partially supported by a U. S. Air Force Office of Scientific Research grant (FA9550-09-1-0622).

References

[1] Shyy, W., Lian, Y., Tang, J., Viieru, D., and Liu, H., *Aerodynamics of Low Reynolds Number Flyers*, Cambridge Univ. Press, New York, 2008.

[2] Dickinson, M. H. and Götz, K. G., "Unsteady Aerodynamic Performance of Model Wings at Low Reynolds Numbers," *Journal of Experimental Biology*, Vol. 174, No. 1, 1993, pp. 45–64.

[3] Ellington, C. P., "The Novel Aerodynamics of Insect Flight: Application to Micro-Air Vehicles," *Journal of Experimental Biology*, Vol. 202, No. 23, 1999, pp. 3439–3448.

[4] Lian, Y., and Shyy, W., "Aerodynamics of Low Reynolds Number Plunging Airfoil Under Gusty Environment," AIAA Paper 2007-0071, Reno, NV, 2007.

[5] Visbal, M. R., "High-Fidelity Simulation of Transitional Flows past a Plunging Airfoil," *AIAA Journal*, Vol. 47, No. 11, 2009, pp. 2685–2697. doi:10.2514/1.43038

[6] Ol, M., "Vortical Structures in High Frequency Pitch and Plunge at Low Reynolds Number," AIAA Paper 2007-4233, 2007.

[7] Williamson, C. H. K., "Vortex Dynamics in the Cylinder Wake," *Annual Review of Fluid Mechanics*, Vol. 28, No. 1, 1996, pp. 477–526. doi:10.1146/annurev.fl.28.010196.002401

[8] Dickinson, M. H., Lehmann, F. O., and Sane, S. P., "Wing Rotation and the Aerodynamic Basis of Insect Flight," *Science*, Vol. 284, No. 5422, 1999, pp. 1954–60. doi:10.1126/science.284.5422.1954

[9] Koochesfahani, M. M., "Vortical Patterns in the Wake of an Oscillating Airfoil," *AIAA Journal*, Vol. 27, No. 9, 1989, pp. 1200–1205. doi:10.2514/3.10246

[10] Ramamurti, R., and Sandberg, W. C., "Simulation of Flow About Flapping Airfoils Using a Finite Element Incompressible Flow Solver," *AIAA Journal*, Vol. 39, No. 2, 2001, pp. 253–260. doi:10.2514/2.1320

[11] Bohl, D. G., and Koochesfahani, M. M., "MTV Measurements of the Vortical Field in the Wake of an Airfoil Pitching at High Reduced Frequency," *Journal of Fluid Mechanics*, Vol. 620, 2009, pp. 63–88. doi:10.1017/S0022112008004734

[12] Lian, Y., and Ol, M., "Experiments and Computation on a Low Aspect Ratio Pitching Flat Plate," AIAA Paper 2010-0385, 2010.

[13] Henshaw, D. W., "A Fourth-Order Accurate Method for the Incompressible Navier–Stokes Equations on Overlapping Grids," *Journal of Computational Physics*, Vol. 113, No. 1, 1994, pp. 13–25. doi:10.1006/jcph.1994.1114

[14] Henshaw, W. D., and Petersson, N. A., "A Split-Step Scheme for the Incompressible Navier–Stokes Equations," *Numerical Simulation of Incompressible Flows*, World Scientific, Hackensack, NJ, 2003, pp. 108–125.

[15] Henshaw, D. W., and Schwendeman, D. W., "Moving Overlapping Grids with Adaptive Mesh Refinement for High-Speed Reactive and Non-Reactive Flow," *Journal of Computational Physics*, Vol. 216, No. 2, 2006, pp. 744–779. doi:10.1016/j.jcp.2006.01.005

[16] Tatsuno, M., and Bearman, P. W., "A Visual Study of the Flow around an Oscillating Circular at Low Keulegan–Carpenter Numbers and Low Stokes Numbers," *Journal of Fluid Mechanics*, Vol. 211, 1990, pp. 157–182. doi:10.1017/S0022112090001537

[17] Dutsch, H., Durst, F., Becker, S., and Lienhart, H., "Low-Reynolds-Number Flow Around an Oscillating Circular Cylinder at Low Keulegan–Carpenter Numbers," *Journal of Fluid Mechanics*, Vol. 360, 1998, pp. 249–271. doi:10.1017/S002211209800860X

[18] Morison, J. R., O'Brien, M. P., Johnson, J. M., and Schaaf, S. A., "The Force Exerted by Surface Waves on Piles," *Petroleum Transactions of AIME*, Vol. 189, 1950, pp. 149–154.

[19] Sarpkara, T., "Vortex Shedding and Resistance in Harmonic Flow About Smooth and Rough Cylinders at High Reynolds Number," Naval Postgraduate School, Rept. NPS-59SL76021, Monterey, CA, 1976.

[20] Uzunoglu, B., Tan, M., and Price, W. G., "Low-Reynolds-Number Flow Around an Oscillating Circular Cylinder Using a Cell Viscous Boundary Element Method," *International Journal for Numerical Methods in Engineering*, Vol. 50, No. 10, 2001, pp. 2317–2338. doi:10.1002/nme.122

P. Beran
Associate Editor